JOURNAL OF MATERIALS SCIENCE **38** (2003) 1695–1702

Dye adsorption behavior of anatase- and rutile-type TiO_2 nanoparticles modified by various heat-treatments

J. TAKAHASHI*
Division of Materials Science and Engineering, Graduate School of Engineering, Hokkaido University, N-13 W-8 Kita-ku, Sapporo 060-8628, Japan
E-mail: tkjun@eng.hokudai.ac.jp

H. ITOH
Department of Materials Science, Kitami Institute of Technology, 165 Koen-cho, Kitami 090-8507, Japan

S. MOTAI, S. SHIMADA
Division of Materials Science and Engineering, Graduate School of Engineering, Hokkaido University, N-13 W-8 Kita-ku, Sapporo 060-8628, Japan

TiO_2 colloidal particles with a fixed crystalline phase of anatase or rutile were heat-treated under different conditions (air-heating and hydrothermal-heating) to modify their surface characters which essentially affected the adsorption behavior of a Ru-complex dye on the surfaces. Changes in the number of surface OH group ($N_{(OH)}$), apparent crystallite size, pore structure were evaluated as a function of heat-treatment conditions for various TiO_2 nanoparticles. The amount of a Ru-complex dye adsorbed ($N_{(dye)}$) was correlated to those surface properties of TiO_2 samples. $N_{(dye)}$ values tended to increase with increasing crystallinity for only the anatase-type TiO_2 particles. However, there was no simple, common relationship between $N_{(dye)}$ and $N_{(OH)}$ for all the TiO_2 nanoparticles examined. Considerable difference in $N_{(dye)}$ values obtained in different nanoparticles might be explained on the basis of the surface pore structures of those particles.

1. Introduction

Nano-sized TiO_2 particles have attracted much attention in the photocatalytic activities since electrochemical photolysis of water at a TiO_2 electrode was reported by Fujishima *et al.* in 1972 [1]. Since then there have been numerous studies of the photocatalytic behavior of nano-sized TiO_2 particles for various applications. Recently, a variety of new products showing an antibacterial effect or deodorization ability are developed, in which the photocatalytic reaction on the TiO_2 surface is effectively combined with some dark reactions [2]. In addition to these applications, dye-sensitized nanocrystalline TiO_2 has been intensively investigated due to potential applicability of constructing a new solar energy conversion system. In 1991, Grätzel and co-workers developed a new kind of solar cell consisting of two electrodes and a redox couple electrolyte between them [3]. One of the electrodes, photoelectrode, was coated with a porous layer of TiO_2 particles, which was sensitized for visible light by adsorbing a dye molecule such as Ru-complexes. Under sun light illumination, the excited electrons in the dye molecule which were produced by adsorbing the solar energy could be injected into the conduction band of the TiO_2 semiconductor. The electrons might drift to the photoelectrode where they could be extracted as an external current. Charge transport between the counterelectrode and the dye molecule was completed through the redox electrolyte.

Although there are many factors affecting the energy conversion efficiency of a dye sensitized solar cell [4–6], a sophisticated TiO_2 nanoparticle is a key material for the optimization of the cell. Among three crystalline phases of TiO_2, anatase is preferred for the semiconducting photoelectrode. This preferential usage could be attributed to its larger band gap ($E_g =$ 3.2 eV and 3.0 eV for anatase and rutile, respectively), which might lead to prolonged performance of the cells [5]. Thus in most of the studies on the dye sensitized TiO_2 solar cell, commercially available P25 titania from Degussa AG (Germany) or colloidal particles derived by hydrolysis of Ti-tetraisopropoxide have been extensively used for the preparation of a porous TiO_2 layer [7–9]. On the other hand, TiO_2 nanoparticles with different surface properties or chemical activities could be

*Author to whom all correspondence should be addressed.

obtained by different preparation methods from various Ti sources [10–13]. Besides, it is not fully understood that what kind of factor in the surface characteristics of TiO_2 nanoparticles would predominate the adsorption behavior of the dye molecule [14–17]. It is important, therefore, to elucidate the fundamental surface properties of such TiO_2 nanoparticles with different crystal structures, anatase and rutile, and to compare their properties for further progress of the dye sensitized solar cell system. The present authors have established the preparation method to obtain separately the anatase type (A-type) and rutile type (R-type) TiO_2 colloid particles [18]. Each particle with the intended crystalline phase could be prepared from an urea-containing $TiCl_4$ solution by controlled thermal hydrolysis of urea. In this study, therefore, both types of the as-precipitated TiO_2 colloids were further heat-treated under various conditions to provide different surface properties for them. Dye adsorption behavior of these heat-treated TiO_2 nanoparticles was examined in relation to the crystalline phase present, crystallinity, and surface properties such as specific surface area, the number of the hydroxyls group, and pore structure.

2. Experimental

2.1. Preparation of colloids and Ru-complex dye

A schematic of the sequence of the colloid preparation procedure with successive heat-treatment is shown in Fig. 1. Fixed amounts of $TiCl_4$ (a concentration of 1.0 mol/dm^3) and urea were dissolved in an aqueous HCl solution (6 mol/dm^3) to form a starting solution. It was heated at 105°C for a given period in a separable flask under N_2 gas flow. The anatase-type (A-type) and rutile-type (R-type) titania colloids were separately prepared by selecting optimum conditions for urea concentration in a starting solution and heating period. The corresponding urea concentration combined with heating time was 16.6 mol/dm^3 with 2 h and 8.8 mol/dm^3 with 8 h for the A- and R-type colloids, respectively [18]. After repeated washing with distilled water, a solution containing a titania colloid with the intended crystalline phase was then heat-treated in different ways. Part of the colloid solution was filtered off and dried at 50°C for 24 h to produce an as-dried titania powder. Fractions of the powdered titania were heat-treated in air at 250, 400, 500, and 700°C for 6 h (air-heating). The remaining part of the colloid solution was heated in a Teflon-lined vessel under hydrothermal conditions at 150°C or 200°C for 48 h (hydrothermal-heating, HT-150 or HT-200).

A Ru-complex dye, cis-$Ru^{II}L_2(NCS)_2$ where $L = 2,2'$-bipyridyl-4,4′-dicarboxylate was synthesized in this study. As the first step, cis-$Ru^{II}L_2Cl_2 \cdot 2H_2O$ was obtained by the method described elsewhere [19]. After this material was prepared, the desired dye molecule was synthesized using the same method as that reported by M. K. Nazeeruddin *et al.* [20]. The production of the dye molecule was confirmed by IR spectroscopy.

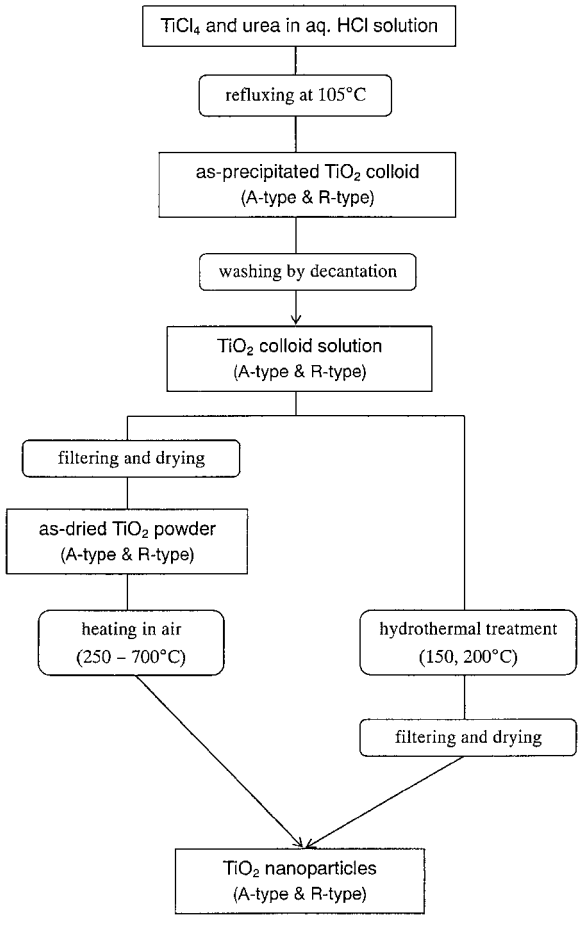

Figure 1 Flow chart for the preparation and heat-treatment of TiO_2 nanoparticles.

2.2. Characterization of TiO_2 nanoparticles

The structural characterization of various TiO_2 nanoparticles was conducted by X-ray powder diffractometry (XRD). Morphology and size of nanoparticles obtained were observed with a transmission electron microscope (TEM). Overall weight loss during heating in air, which might be due to dehydration and/or release of some chemical species adsorbed on the surface or absorbed in the particle was measured by TG-DTA analysis. Specific surface area per unit mass (Sw) of a powder sample together with pore size distribution was estimated by BET N_2 gas adsorption method.

Surface hydroxyl group concentration of a heat-treated sample was measured by the reaction with triethylaluminium ($Al(C_2H_5)_3$, TEA). A powder sample to be measured was placed in a reactor and heated under vacuum at 250°C for 12 h. After the evacuation, N_2 gas was introduced up to an atmospherics pressure and a solution of TEA in pure, deoxygenated Decaline was poured with a syringe through a rubber cap. Hydroxyl groups on the sample surface then reacted with TEA to yield ethane according to the equation $M\text{-}OH + Al(C_2H_5)_3 \rightarrow M\text{-}O\text{-}Al(C_2H_5)_2 + C_2H_6$. The amount of ethane molecules thus produced could be quantified by detecting the mercury level change in a gas burette. The validity of this method has been confirmed in a study on the estimation of surface hydroxyl content of ultrafine MgO particles [21].

The adsorption of the Ru-complex dye on a sample surface was conducted using the same apparatus

as that used for measuring surface OH group to avoid the effect of some impurity species adsorbed on the surface. After evacuation at 250°C and N_2 gas introduction in the system, a solution of cis-$Ru^{II}L_2(NCS)_2$ in ethyl alcohol (a concentration of 6×10^{-4}mol/dm^3) was poured into a reactor where a sample powder had been already set. The reactor which contained a powder sample together with the dye solution was repeatedly ultrasonicated in every 4 h interval up to 24 h. The amount of the dye adsorbed was measured by a change of dye concentration in ethanol before and after the adsorption operation. A dye-adsorbed titania particle was separated from an original ethanol solution by pressure filtration. The concentration of the remaining dye molecule in a filtrate was analyzed by absorption spectrophotometry. The amount of the Ru-complex dye molecule adsorbed per unit surface area of titania nanoparticles (N_{dye}[number/nm^2]) was calculated from the equation below.

$$N_{dye} = \frac{V_{dye}\left(C^0_{dye} - C_{dye}\right)Av}{W \cdot Sw} \times 10^{-18}\,[1/nm^2]$$

where C^0_{dye} and C_{dye} are the concentrations of Ru-complex solutions before and after adsorption [mol/dm^3], respectively, V_{dye} the amount of Ru-complex solution injected [dm^3], W the mass of a titania powder to be examined [g], Sw the specific surface area of the titania sample (m^2/g), and Av Avogadro number (6.02×10^{23}/mol).

3. Results and discussion

3.1. Changes in particle morphology and crystallinity with heat-treatments

Fig. 2(1) and (2) show XRD patterns of TiO_2 powders with the A-type and R-type structures, respectively. As-precipitated particles, (a) in Fig. 2(1) and (2), were heated in air at 250°C (b), 500°C (c) and also hydrothermally treated at 150°C (d) and 200°C (e). Broadened XRD peaks of the as-precipitated A-type particles showing very low crystallinity progressively become sharpened with increasing air-heating temperature. A marked increase in crystallinity was recognized after hydrothermal-heating. The changes in crystallinity for those treated particles are quantitatively presented in Fig. 3 as apparent crystallite size (Lapp) variation, in which Lapp was calculated from broadening of XRD peaks. It is obvious that the Lapp of the A-type HT150 sample is comparable to that of TiO_2 particles by air-heating at 500°C. Besides, a very small crystallite size of the as-precipitated A-type particles (~4 nm) substantially increases by a factor of 6 after hydrothermal-heating at 200°C. This change can be confirmed by TEM observation in Fig. 4 where the extremely small as-prepared anatase colloids (a) and the well-crystallized, idiomorphic A-type TiO_2 nanoparticles produced by hydrothermal treatment ((c) and (d)) are clearly seen. As has been pointed out [5], an advantage of the hydrothermal treatment is to yield well formed crystals with low defect density. Therefore, it has been commonly employed to modify TiO_2 colloid particles in a lot of studies of their photocatalytic applications. Bipyramidal morphology observed in the

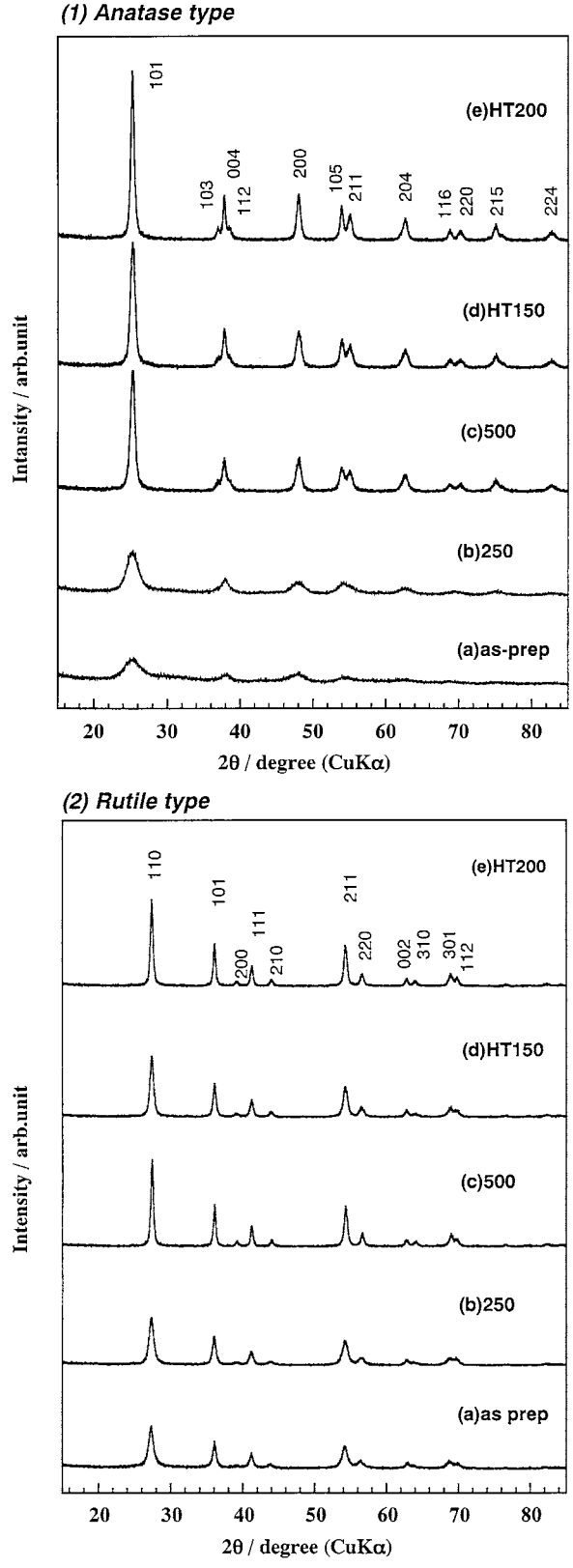

Figure 2 XRD patterns of as-precipitated and heat-treated TiO_2 nanoparticles with (1) A-type and (2) R-type structures.

A-type HT200 particles (Fig. 4d) is very similar to that of TiO_2 particles which was autoclaved at 250°C in ammonia at pH = 11 [16]. Since the presence of NH_3 group was detected by IR spectroscopy of both the as-precipitated colloids and HT200 particles, a certain amount of ammonia adsorbed in the precipitation process could not be completely removed from the as-precipitated colloids by repeated washing with distilled

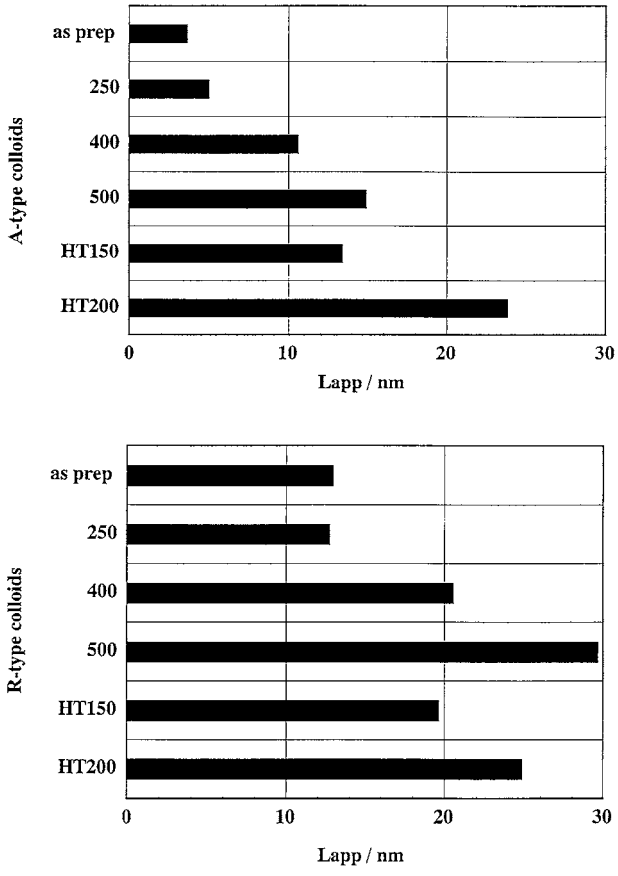

Figure 3 Apparent crystallite sizes of various TiO_2 particles.

water. The adsorbed ammonia could produce a basic environment under hydrothermal conditions, leading to the growth of the bipyramidal TiO_2 nanoparticles.

For the R-type particles prepared under various conditions, on the contrary, some different characteristics were clearly demonstrated in Figs 2(2), 3 and 5. First, apparent crystallite size of the as-precipitated particles was much larger than that of the A-type colloid. The production of the R-type nanoparticles with better crystallinity might be partly due to prolonged heating in the preparation process [18]. Secondary, comparing the Lapp changes between each type sample, autoclaving for the R-type titania particles was not so effective as that observed for the A-type sample. As clearly seen in Fig. 5, there was basically little change in the shape of the R-type secondary particles with lamella structure (strips of elongated particles), especially for hydrothermally treated samples. Elongation and aggregation of the R-type secondary particles were correspondingly accelerated by both treatments with a resulting increase in crystallinity.

3.2. Surface properties affecting dye adsorption behavior

The adsorption characteristic of the dye molecule on various TiO_2 nanoparticles was basically examined in relation to surface OH group. Table I summaries specific surface area (Sw), weight loss by means of TG measurement, and the number of surface OH group ($N_{(OH)}$) per unit mass for both A- and R-type TiO_2 particles treated under various conditions. It also contains the number of dye molecule ($N_{(dye)}$) adsorbed on each particle on unit mass and unit surface area bases. Weight loss shown with bracketed numerals in Table I, (TG), corresponded to that in the temperature region 250–800°C. Since TG measurement was conducted for samples treated under the specified conditions (i.e., air-heating or hydrothermal-heating at different temperatures), bracketed numerals would be associated with the loss of chemically bonded OH group and/or other molecules sorbed in the particles. Relatively larger values obtained for hydrothermally-treated samples (A-HT200 and R-HT200) might be attributed to adsorbed NH_3 molecules as described in the previous sections.

Concerning the adsorption behavior of Ru-complexes on TiO_2 particles, Falaras has investigated the surface interaction of TiO_2 particles (Degussa P25) with some selected Ru-complexes with −COOH functional group by FTIR spectroscopy [17]. He found that the dye molecules were chemically adsorbed onto the TiO_2 particles via formation of ester-like binding between the carboxylic acid groups and OH groups on TiO_2. In addition to this kind of binding, the dye molecules might adhere to TiO_2 particles by hydrogen bonding to the surface OH groups. Thus the surface OH groups should be closely interrelated with the amount of dye adsorbed. To examine a relationship between them on TiO_2 particles prepared in the present study, $N_{(OH)}$ in Table I, which was determined by the quantitative reaction between TEA and surface OH group, could be re-estimated on an unit surface basis (100 nm^2) and plotted in Fig. 6 with the corresponding $N_{(dye)}$ change. Ti ion sites on the surface of TiO_2 particles to which OH group would bind can be theoretically estimated to be 541 and 762 per 100 nm^2 of the anatase and rutile phase, respectively. These values are the average of four representative crystal planes, (100), (001), (110) and (011). It was obvious from the measured values in Fig. 6 that those measured OH groups were chemically adsorbed on the surface of each sample after various heat-treatments and the number of the chemisorbed OH group roughly corresponded to one fourth or one fifth of the theoretical Ti ion sites. For the A-type samples, various heat-treatments of the as-precipitated nanoparticles caused only a slight change in the amount of the chemisorbed OH group between the samples examined. On the other hand, a relatively large variation in the chemisorbed OH group was observed in the R-type nanoparticles. A tendency for the surface OH group to decrease with an increase in heating temperature is commonly recognized for oxide particles. Therefore, a change in the $N_{(OH)}$ values obtained for the A-type particles was rather peculiar, although it was unclear what kind of causes would bring about the different changes between both types of TiO_2 particles.

As clearly seen in Fig. 6, there is no simple relationship between $N_{(OH)}$ and $N_{(dye)}$ for the A- and R-type TiO_2 nanoparticles. However, since the $N_{(dye)}$ values seemed to gradually increase with heating temperature for both samples, the dye adsorption might be correlate with the crystallinity change of TiO_2 particles. Then the $N_{(dye)}$ values are plotted as a function of apparent crystallite size in Fig. 7. For TiO_2 particles

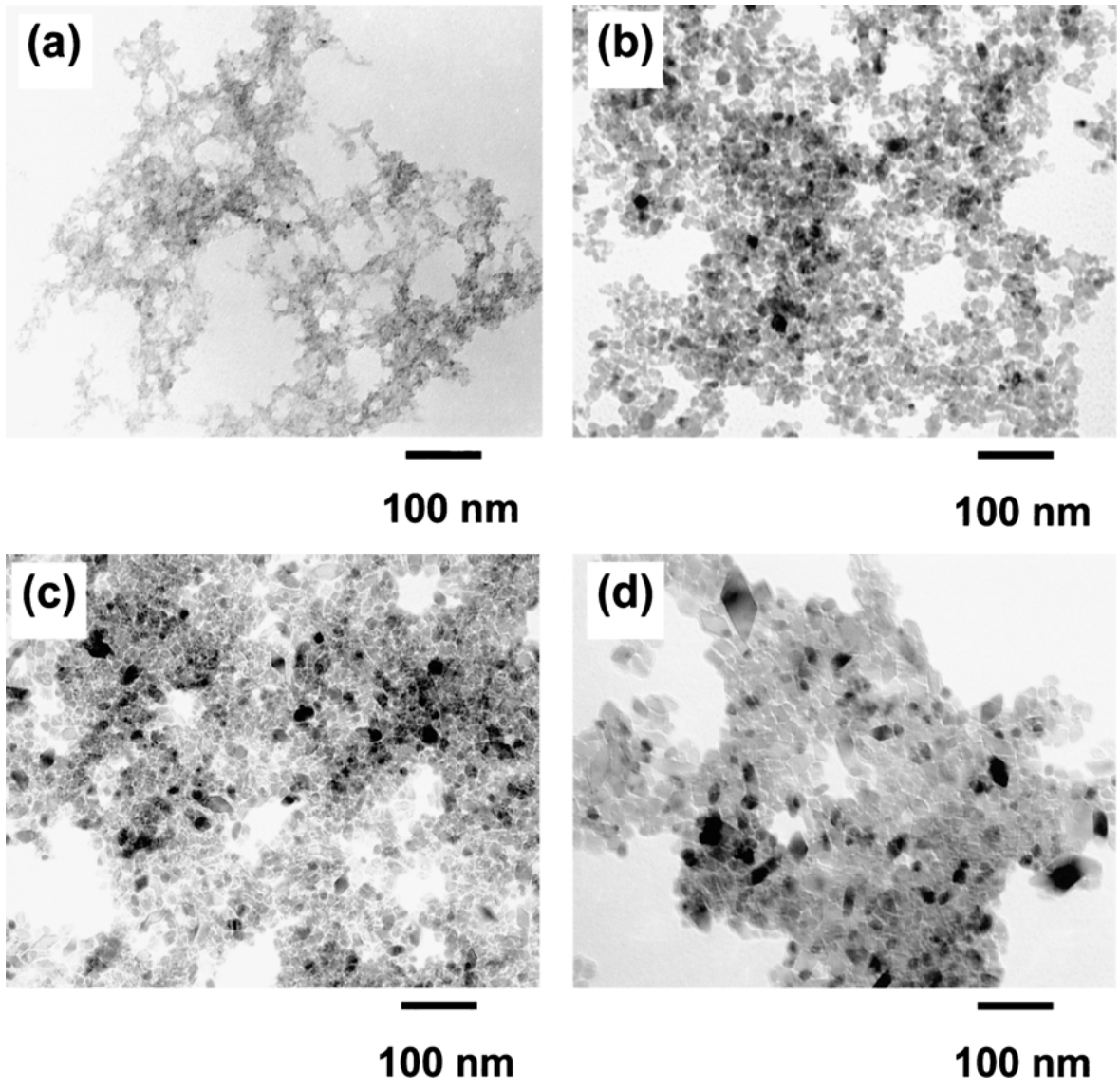

Figure 4 TEM images of the A-type samples; (a) as-precipitated, (b) air-heating at 500°C, and (c), (d) hydrothermal-heating at 150°C and 200°C, respectively.

with their crystallite size less than 40 nm, the amount of dye adsorbed increased with the increasing Lapp for both samples. The R-type particles heat-treated at higher temperatures, however, were found to have much smaller $N_{(dye)}$ values. This indicated that there was apparently no simple and definite relationship between them.

Fig. 8 shows the pore size distribution curves of selected TiO_2 samples with considerably different amounts of dye adsorbed. Their measured $N_{(dye)}$ values are given in Table I with that of commercial P25 sample (A-P25) for comparison. It was obvious that those particles have own characteristic pore structures. The A-400 particles contained a huge number of small pores less than about 4 nm, whereas the pore size in the hydrothermally treated A-HT200 sample mostly ranged from 4 nm to 8 nm. On the contrary, the A-P25 particles revealed a substantially different pore structure consisting of much larger pores with their radii ranging from 15–40 nm. Among these samples, the highest $N_{(dye)}$ value was observed in the A-P25 sample composing of the largest pores, while the lowest $N_{(dye)}$ value was for the A-400 sample with a large number of very small pores. Since the Ru-complex dye used in this study is a substantially large molecule with its diameter of about 1.7 nm [15], they could not enter into smaller pores. Therefore, a smaller $N_{(dye)}$ value of the A-400 sample might be due to overestimation of specific surface area available for the dye adsorption and would become a larger $N_{(dye)}$ value by re-estimation on a reduced Sw basis. The measured $N_{(dye)}$ values of the A-HT200 and A-P25 samples, on the other hand, could be appropriately estimated because they have differently sized pores with their radii being larger than $\sim$4 nm. Assuming that the dye molecule adsorbed via formation of ester-like linkage sterically occupies an area of about 2×2 nm^2 per a molecule on the TiO_2 surface, the number of the adsorbed dye molecule could be theoretically calculated to be $\approx$25 per 100 nm^2 for monolayer coverage. The measured $N_{(dye)}$ value of the R-700 sample without any detectable pores, 17/100 nm^2, was rather less than that based on the above assumption. On the other hand, the $N_{(dye)}$ values of the A-HT200 and A-P25 samples are much larger than the calculated one, suggesting

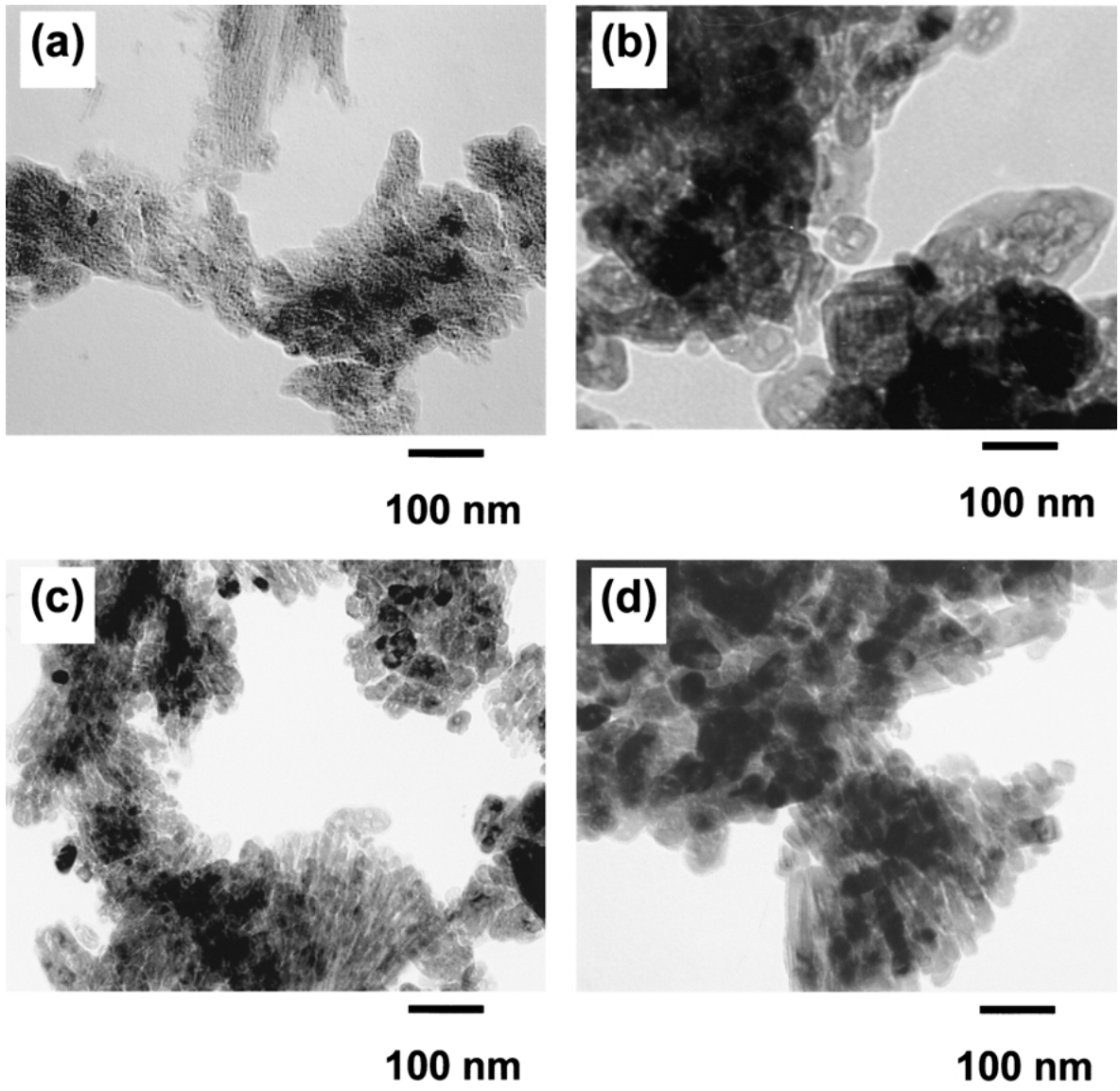

Figure 5 TEM images of the R-type samples; (a) as-precipitated, (b) air-heating at 500°C, and (c), (d) hydrothermal-heating at 150°C and 200°C, respectively.

the occurrence of multilayer coverage of the dye molecule.

From above results, the adsorption behavior of the Ru-complex might be strongly affected by the degree of crystallinity and pore structure (porosity and pore size distribution) of the surface of TiO_2 nanoparticles. That is, for samples treated by air-heating at lower temperatures, low crystallinity and small pore size should lead to a reduced surface area available for the dye adsorption (although measured Sw was much larger) and accordingly result in an apparent decrease in $N_{(dye)}$. When a sample was air-heated at higher temperatures

TABLE I Specific surface area, weight loss, and the numbers of surface OH group and dye molecule adsorbed for various TiO_2 nanoparticles

Sample	Sw (m^2/g)	Weight loss (TG2) (%)	$N_{(OH)}$ (n × 10^{19}/g)	$N_{(dye)}$ (n × 10^{18}/g)	$N_{(dye)}$ (n/100 nm^2)
A-250	420	11.0 (3.8)	50.4	53.3	12.7
A-400	201	—	23.7	40.2	20.2
A-500	148	2.80 (0.50)	16.3	31.8	21.5
A-HT150	145	—	16.8	32.2	22.2
A-HT200	97	3.48 (0.78)	12.5	41.9	43.2
(A-P25)	(63)	—	(9.5)	(44.5)	(70.7)
R-250	86	3.10 (1.10)	11.3	17.9	20.8
R-400	65	—	5.8	16.7	25.7
R-500	31	0.46 (0.22)	2.8	9.6	31.1
R-700	6.5	—	0.046	1.1	16.8
R-HT150	80	—	11.5	31.1	38.9
R-HT200	52	2.30 (1.10)	8.1	25.7	49.4

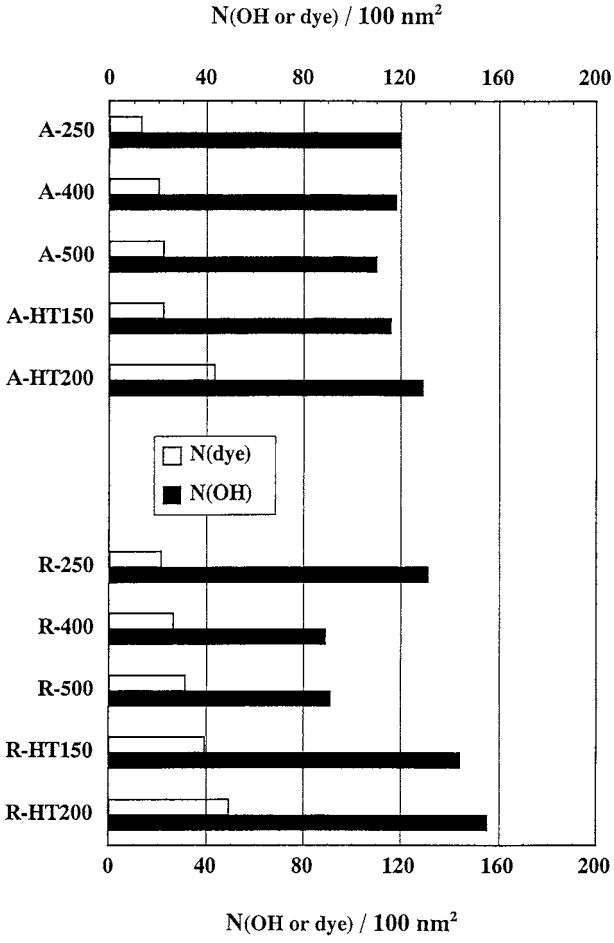

Figure 6 $N_{(OH)}$ and $N_{(dye)}$ for the A- and R-type TiO_2 nanoparticles.

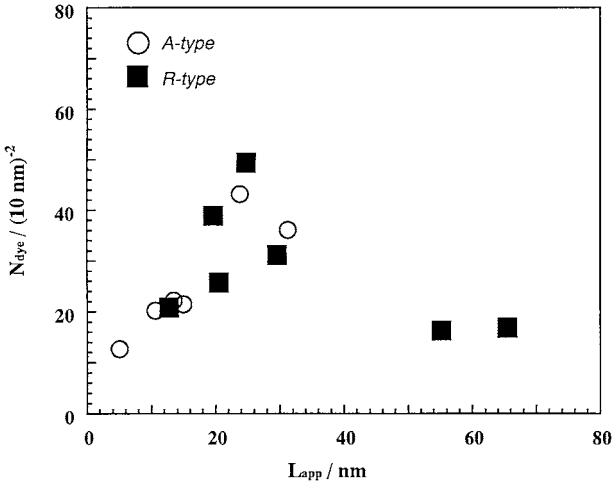

Figure 7 Relationship between $N_{(dye)}$ and Lapp for various particles examined.

or hydrothermally treated, pore growth occurred with elimination of smaller pores, while the crystallinity of the particles increased. For these particles (A-P25 also), the multilayer coverage might occur on a flat surface of TiO_2 nanoparticles under the experiment conditions employed in this study. In general, the multilayer coverage of the dye molecule should be avoided for the practical use of TiO_2 nanoparticle-based solar cell system. In the present study, it was interesting that the monolayer or sub-monolayer coverage was observed only for the R-type particles without appreciable pores. Therefore,

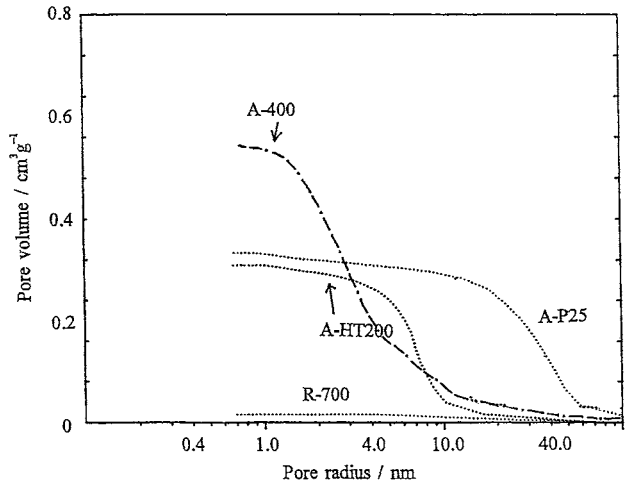

Figure 8 Pore size distributions for some selected TiO_2 particles.

further study has to be done for detailed understanding of the adsorption behavior of the dye molecule on TiO_2 nanoparticles.

4. Conclusions

TiO_2 nanoparticles with different crystalline phases, anatase (A-type) and rutile (R-type), which were separately prepared using thermal hydrolysis of urea were successively heat-treated under different conditions to provide different surface characteristics of the particles. Adsorption behavior of a Ru-complex dye was studied for those TiO_2 nanoparticles in relation to crystalline phase, crystallinity and their surface properties such as the number of OH group adsorbed and pore structure. The results obtained were as follows;

1. The particle size, shape and crystallinity were substantially modified by hydrothermal-heating for the A-type colloids, whereas gradual increases or improvement in those properties were observed for the R-type colloids.
2. The number of OH group adsorbed on the surfaces of TiO_2 nanoparticles, $N_{(OH)}$, heat-treated under various conditions ranged 90–145 per unit surface area (100 nm^2), which were independent on the heating conditions.
3. Concerning the A-type TiO_2 nanoparticles only, the amount of the dye adsorbed, $N_{(dye)}$, tended to increase with increasing crystallinity.
4. However, there was no simple, common relationship between $N_{(OH)}$ and $N_{(dye)}$ for all the TiO_2 nanoparticles examined.
5. Considerably different $N_{(dye)}$ values measured for different kinds of nanoparticles might be explained by taking into account the pore structures of those samples.

References

1. A. FUJISHIMA and K. HONDA, *Nature* **238** (1972) 37.
2. K. HASHIMOTO and A. FUJISHIMA, *Bull. Ceram. Soc. Jpn.* **31** (1996) 815 (In Japanese).
3. B. O'REAGAN and M. GRÄTZEL, *Nature* **353** (1991) 737.
4. G. SMESTAD, C. BIGNOZZI and R. ARGAZZI, *Sol. Energy Mater. Sol. Cells* **32** (1994) 259; G. Smestad, *ibid.* **32** (1994) 273.
5. A. KAY and M. GRÄTZEL, *ibid.* **44** (1996) 99.
6. J. FERBER, R. STANGL and J. LUTHER, *ibid.* **53** (1998) 29.

7. R. HOYLE, G. WILL and D. FITZMAURICE, *J. Mater. Chem.* **8** (1998) 2033.
8. Y. LI, J. HAGEN, W. SCHAFFRATH, P. OTSCHIK and D. HAARER, *Sol. Energy Mater. Sol. Cells* **56** (1999) 167.
9. S. KAMBE, K. MURAKOSHI, T. KITAMURA, Y. WADA, S. YANAGIDA, H. KOMINAMI and Y. KERA, *ibid.* **61** (2000) 427.
10. J. RAGAI and K. S. W. SING, *J. Colloid Interface Sci.* **101** (1984) 369.
11. E. SANTACESARIA, M. TONELLO, G. STORTI, R. C. PACE and S. CARRA, *ibid.* **111** (1986) 44.
12. F. CAVANI, E. FORESTI, F. PARRINELLO and F. TRIFIRÒ, *Appl. Catal.* **38** (1988) 311.
13. K. R. LEE, S. J. KIM, J. S. SONG, J. H. LEE, Y. J. CHUNG and S. J. PARK, *J. Amer. Ceram. Soc.* **85** (2002) 341.
14. K. MURAKOSHI, G. KANO, Y. WADA, S. YANAGIDA, H. MIYAZAKI, M. MATSUMOTO and S. MURASAWA, *J. Electroanal. Chem.* **396** (1995) 27.
15. V. SHKOVER, M.-K. NAZEERUDDIN, S. M. ZAKEERUDDIN, C. BARBÉ, A. KAY, T. HAIBACH, W. STEURER, R. HERMANN, H.-U. NISSEN and M. GRÄTZEL, *Chem. Mater.* **9** (1997) 430.
16. C. J. BARBÉ, F. ARENDSE, P. COMTE, M. JIROUSEK, F. LENZMANN, V. SHKLOVER and M. GRÄTZEL, *J. Amer. Ceram. Soc.* **80** (1997) 3157.
17. P. FALARAS, *Sol. Energy Mater. Sol. Cells* **53** (1998) 163.
18. J. TAKAHASHI, H. SUZUKI and K. KODAIRA, *J. Sol-Gel Sci. Technol.* **4** (1995) 15.
19. P. LISKA, N. VLACHOPOULOS, M. K. NAZEERUDDIN, P. COMTE and M. GRÄTZEL, *J. Amer. Chem. Soc.* **110** (1988) 3686.
20. M. K. NAZEERUDDIN, A. KAY, I. RODICIO, R. HUMPHRY-BAKER, E. MÜLLER, P. LISKA, N. VLACHOPOULOS and M. GRÄTZEL, *ibid.* **115** (1993) 6385.
21. H. ITOH, S. UTAMAPANYA, J. V. STARK, K. J. KLABUNDE and J. R. SCHLUP, *Chem. Mat.* **5** (1993) 71.

Received 3 June 2002
and accepted 21 January 2003